# optica

# Quantum teleportation over 100 km of fiber using highly efficient superconducting nanowire single-photon detectors

Hiroki Takesue,[1,*] Shellee D. Dyer,[2] Martin J. Stevens,[2] Varun Verma,[2] Richard P. Mirin,[2] and Sae Woo Nam[2]

[1]NTT Basic Research Laboratories, NTT Corporation, 3-1 Morinosato Wakamiya, Atsugi, Kanagawa 243-0198, Japan
[2]National Institute of Standards and Technology, 325 Broadway, Boulder, Colorado 80305, USA
*Corresponding author: takesue.hiroki@lab.ntt.co.jp

**Quantum teleportation is an essential quantum operation by which we can transfer an unknown quantum state to a remote location with the help of quantum entanglement and classical communication. Since the first experimental demonstrations using photonic qubits and continuous variables, the distance of photonic quantum teleportation over free-space channels has continued to increase and has reached >100 km. On the other hand, quantum teleportation over optical fiber has been challenging, mainly because the multifold photon detection that inevitably accompanies quantum teleportation experiments has been very inefficient due to the relatively low detection efficiencies of typical telecom-band single-photon detectors. Here, we report on quantum teleportation over optical fiber using four high-detection-efficiency superconducting nanowire single-photon detectors (SNSPDs). These SNSPDs make it possible to perform highly efficient multifold photon measurements, allowing us to confirm that the quantum states of input photons were successfully teleported over 100 km of fiber with an average fidelity of $83.7 \pm 2.0\%$.**    © 2015 Optical Society of America

In the last two decades, we have seen remarkable progress in quantum key distribution (QKD) over optical fiber [1,2]. QKDs over >100 km of fiber have been achieved with schemes based on attenuated laser light [3–5] and entanglement distribution [6]. However, to overcome the exponential decrease in the key rate caused by fiber loss and to achieve scalable QKD, we will need a quantum repeater [7,8], in which quantum teleportation [9] plays a crucial role.

Since the first experimental demonstrations using photonic qubits [10] and continuous variables [11] over very short distances on optical tables, the distance of quantum teleportation over free-space channels has continued to increase and has reached >100 km [12,13]. On the other hand, quantum teleportation over optical fiber has been challenging [14,15], mainly because the multifold photon detection that inevitably accompanies quantum teleportation experiments has been very inefficient due to the relatively low detection efficiencies of typical telecom-band single-photon detectors. Consequently, there have been relatively few reports of quantum teleportation over optical fiber [14,15]. In the pioneering experiment reported in [14], the quantum states of time-bin qubits were transferred over 2 km of fiber. A recent experiment [15], which set the record distance for quantum teleportation over fiber (25 km), implemented a quantum relay configuration with the teleported photon stored in a quantum memory. Recently, superconducting nanowire single-photon detectors (SNSPDs) with >90% detection efficiency in the 1.5 μm band have been realized using superconducting nanowires made of amorphous tungsten silicide (WSi) [16]. In the present work, we employed SNSPDs based on another amorphous material, molybdenum silicide (MoSi), to perform photonic quantum teleportation over fiber. The choice of MoSi instead of WSi allowed operation at a higher temperature with less jitter [17]. We used four high-detection-efficiency (80%–86%) MoSi SNSPDs, which enabled us to perform highly efficient multifold coincidence measurements, resulting in the successful quantum teleportation over 100 km of fiber.

Here, we describe the setup of our quantum teleportation experiment. As a quantum information carrier, we use a photon encoded as a time-bin qubit, which is a coherent superposition of two temporal modes [18]. A photonic time-bin qubit is more suitable for fiber transmission than a polarization qubit because it is generally difficult to preserve a polarization state in a long fiber. Figure 1(a) shows the configuration of the time-bin entangled photon pair source. Subpicosecond pulses from a fiber mode-locked laser with a repetition frequency of 35.53 MHz are passed through a wavelength filter whose center wavelength and bandwidth are 1551.1 nm and 20 GHz, respectively. As a result, we obtain pulses with a temporal width of ~20 ps. The pulses are launched into an unbalanced Mach–Zehnder interferometer (MZI) whose delay time is 1 ns to create double pulses.

The double pulses are amplified by an erbium-doped fiber amplifier and launched into the first periodically poled lithium niobate (PPLN) waveguide, where a pump pulse train with a wavelength of 775.6 nm is generated via the second-harmonic generation process. The 775.6 nm pulses are then passed through a filter to eliminate the 1551.1 nm light and input into the second PPLN waveguide, where time-bin entangled photon pairs whose state is given by $|\psi\rangle = (|1\rangle_s|1\rangle_i + |2\rangle_s|2\rangle_i)/\sqrt{2}$ are generated through the spontaneous parametric downconversion process. Here, $|x\rangle_y$ denotes a state where there is a photon at a time slot $x$ in a mode $y$. The generated photon pairs are separated into signal (1546.3 nm) and idler (1555.9 nm) channels using a wavelength filter with a transmission bandwidth of 20 GHz for both channels, resulting in a photon pair coherence time of ~20 ps. To prepare an input qubit whose wavelength is the same as that of the signal photon, a portion of the output from the fiber mode-locked laser (before spectral filtering) is extracted by a 99:1 fiber coupler, passed through an attenuator to make the average photon number per pulse much less than 1, and then launched into an optical bandpass filter whose wavelength and transmission bandwidth are exactly the same as those used for separating signal photons. The output attenuated laser pulse is input into another unbalanced interferometer (MZI1) whose delay time is 1 ns to create a time-bin qubit for use as an input photon. Our unbalanced interferometers are based on a silica waveguide. The phase differences between the two waveguide arms are stably controlled by tuning the waveguide temperature [19]. In the following teleportation experiment, we set the average photon number per qubit for the entangled photon pairs and the input photons at 0.016. The characteristics of the time-bin entangled photon pair source are described in Supplement 1.

The setup for our quantum teleportation experiment is shown in Fig. 1(b). The signal and input photons are passed through polarization controllers and then launched into a 3 dB fiber coupler followed by SNSPD1 and SNSPD2. Here, the temporal distinguishability between the two photons is eliminated by adjusting the temporal position of the input photon using a variable delay line, while the polarization distinguishability is eliminated by adjusting the polarization controllers to maximize the number of photons that passed through a polarizer placed in front of SNSPD1. We can project the two photons into $|\Psi^-\rangle$ by

conditioning on events where both SNSPD1 and SNSPD2 detect photons but in different time slots, as described in Supplement 1. The idler photon is transmitted over 102 km of dispersion-shifted fiber, and is received by another unbalanced interferometer (MZI2) whose two output ports are connected to SNSPD3 and SNSPD4. The loss of the 102 km fiber was 21.8 dB, including connector losses. Note that the 102 km fiber was wound in coils, and the physical separation between the time-bin entanglement source and MZI2 was a few meters. Thanks to the narrow bandwidth of the idler photon, the temporal waveform broadening caused by higher-order dispersion in a fiber is negligibly small. The detection signals from the SNSPDs are received by a time interval analyzer (TIA) for coincidence measurements. By conditioning the detection events at SNSPD3 or SNSPD4 on the successful projection of the signal and input photons to $|\Psi^-\rangle$, we can teleport the quantum state of an input photon to that of the idler photon with a predetermined unitary transformation.

It should be noted that we can implement two nonorthogonal measurements using MZI2 followed by two single-photon detectors [20,21]. Let us denote the phase difference between the two arms of MZI2 by $\theta_2$. When a time-bin qubit passes through MZI2, the detectors can possibly detect a photon in three time slots. The detection of a photon in the second time slot with SNSPD3 and SNSPD4 means that the input qubit is projected to the states $(|1\rangle + e^{i\theta_2}|2\rangle)/\sqrt{2}$ and $(|1\rangle - e^{i\theta_2}|2\rangle)/\sqrt{2}$, respectively. On the other hand, when we detect a photon in the first or third time slots with either of the detectors, the qubit is projected to state $|1\rangle$ or $|2\rangle$, respectively. Hereafter, we refer to a projection measurement at the second slot as a superposition-basis measurement, and that at the first or third slots as a time-basis measurement.

The system detection efficiencies of the SNSPDs were 80% (SNSPD1), 86% (SNSPD2 and SNSPD3), and 81% (SNSPD4), while the background count rates were ~$10^2$ cps for all the detectors. The timing jitter of the SNSPDS was ~90 ps, and thus the measurement errors caused by intersymbol interference were negligible in our experiment where the temporal difference between time bins was 1 ns. The SNSPDs are described in detail in Supplement 1.

We performed a Hong–Ou–Mandel (HOM) interference experiment to investigate the indistinguishability of the input and
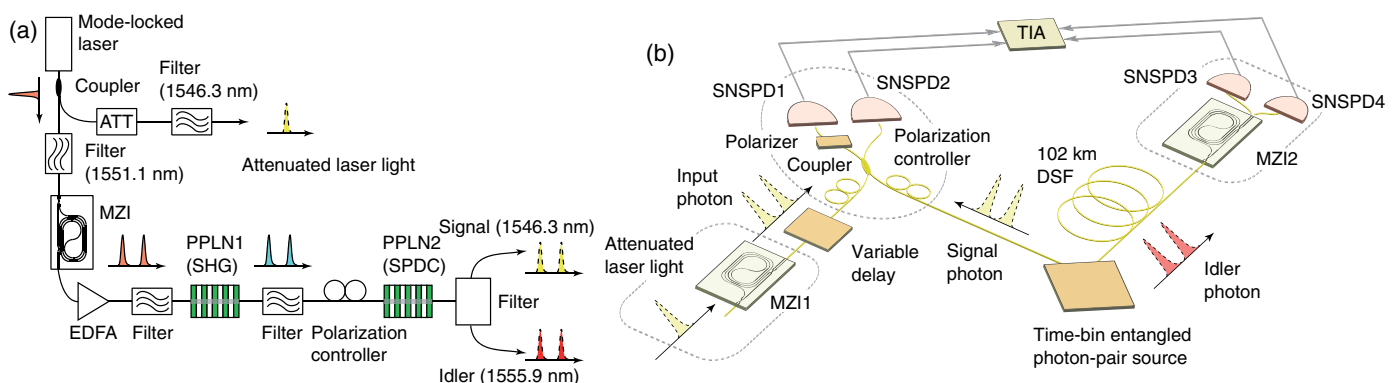


**Fig. 1.** Experimental setup. (a) Setup for generating time-bin entangled photon pairs. ATT, attenuator; EDFA, erbium-doped fiber amplifier; PPLN, periodically poled lithium niobate waveguide; SHG, second-harmonic generation; SPDC, spontaneous parametric downconversion. (b) Quantum teleportation setup. Yellow and gray solid lines indicate the optical fibers and electrical lines, respectively. SNSPD, superconducting nanowire single-photon detector; MZI, unbalanced Mach–Zehnder interferometer; DSF, dispersion-shifted fiber; TIA, time interval analyzer.

the signal photons [22]. We removed the transmission fiber and MZIs, and the idler photons were directly received by SNSPD3. We observed the HOM interference by taking the triple coincidences between SNSPD1, SNSPD2, and SNSPD3 as a function of relative delay between the input and signal photons. Note that this experiment corresponds to quantum interference between an attenuated laser pulse and a heralded single photon, and the theoretical limit of the visibility moves closer to 100% when the average number of the input photons per pulse is decreased and when the background counts of the detectors are negligible [23]. The result is shown in Fig. 2(a). At zero relative delay, we observed a clear dip in the triples. The visibility of the HOM dip was $76.9 \pm 3.4\%$, which significantly exceeded the classical limit of HOM visibility of 50%. Since the pump pulse width and the coherence time of the photon pairs were similar in our experiment, the remaining frequency correlation between the entangled photons is expected to be the main source of visibility reduction from 100%.

We then performed a quantum teleportation experiment. We first removed the transmission fiber from the setup shown in Fig. 1. We launched input photons whose state is given by $(|1\rangle + e^{i\theta_1}|2\rangle)/\sqrt{2}$ by setting the MZI1 phase at $\theta_1$, and observed the photon-detection events with SNSPD3 and SNSPD4 in the superposition basis conditioned on the projection of the signal and input photons to $|\Psi^-\rangle$. The result is shown in Figs. 2(a) (SNSPD3) and 2(b) (SNSPD4). Thus, we confirmed that the phase of the input photon was successfully transferred to that of the idler photon. The visibilities were $60.5 \pm 5.0\%$ for the SNSPD3 channel and $57.5 \pm 5.7\%$ for the SNSPD4 channel. Note that we did not subtract any accidental coincidences or background counts from any of the experimental data shown in this Letter. In this experiment, the limited HOM visibility induced the errors in the Bell state measurement, resulting in the reduction in fringe visibility from 100%.

We then performed a quantum teleportation experiment over 100 km of fiber for six distinct input states. We prepared states $|\pm\rangle = (|1\rangle \pm |2\rangle)/\sqrt{2}$, $|L\rangle = (|1\rangle + i|2\rangle)/\sqrt{2}$, and $|R\rangle = (|1\rangle - i|2\rangle)/\sqrt{2}$ by adjusting the MZI1 phase $\theta_1$, while the other two states $|1\rangle$ and $|2\rangle$ were obtained by removing MZI1 and adjusting the temporal positions of the qubits so that they coincided with that of the first and second pulses of the signal photons, respectively. Note that in our quantum teleportation experiment, the input photon states $|1\rangle$, $|2\rangle$, $|L\rangle$, $|R\rangle$, and $|\pm\rangle$ are transformed to the idler photon states $|2\rangle$, $|1\rangle$, $|L\rangle$, $|R\rangle$, and $|\mp\rangle$, respectively

(see Supplement 1 for details). We undertook quantum state tomography (QST) [24] on the teleported states to obtain their density matrices. We employed six projection measurements that correspond to $|\pm\rangle$, $|L\rangle$, $R\rangle$, $|1\rangle$, and $|2\rangle$ to perform QST on a single qubit. The projections to $|+\rangle$ and $|-\rangle$ were achieved by performing superposition-basis measurements with $\theta_2 = 0$ at SNSPD3 and SNSPD4, respectively, while the $|L\rangle$ and $|R\rangle$ projections were implemented by employing superposition-basis measurements at SNSPD3 and SNSPD4, respectively, with $\theta_2 = \pi/2$. The projections to $|1\rangle$ and $|2\rangle$ were achieved with time-basis measurements at the first and third time slots, respectively. Since our setup was inherently equipped with two nonorthogonal measurement bases, we could perform the six projections with only two TIA measurements at $\theta_2 = \{0, \pi/2\}$ [21]. The data acquisition time for each TIA measurement was 6000 s, which means that the total QST measurement time for each input state was 12,000 s. The average number of triple coincidences for each basis was ~170. With the raw data obtained in the QST measurements, we performed a maximum likelihood estimation to obtain physically legitimate matrices [24]. The reconstructed density matrices after the maximum likelihood estimation are provided in Supplement 1. Using these density matrices, we calculated the fidelity for each input state. The results are shown in Fig. 3. We obtained an average fidelity of $83.7 \pm 2.0\%$ for the six distinct input states, which means that we observed a violation of the classical limit (66.7%) by more than eight standard deviations.

If we assume that the state of the teleported photon is a Werner state, the fidelity $F$ and the fringe visibility $V$ are related as $F = (1 + V)/2$. This means that the fidelity of the teleportation without a 100 km fiber shown by Figs. 2(b) and 2(c) is ~80%. Thus, we observed no fidelity degradation induced by the 100 km fiber transmission of the idler photons, thanks to the low noise characteristics of the SNSPDs.

In the quantum teleportation experiment over a 100 km fiber, we observed a significant drift in the temporal position of the teleported photons which is caused by the fiber length fluctuation induced by changes in the room temperature. Therefore, we implemented a scheme to monitor the drift for the stable counting of the triple coincidences (see Supplement 1 for details).

We have achieved a quantum teleportation distance similar to those achieved in previous experiments performed on free-space channels [12,13]. In those experiments, quantum states
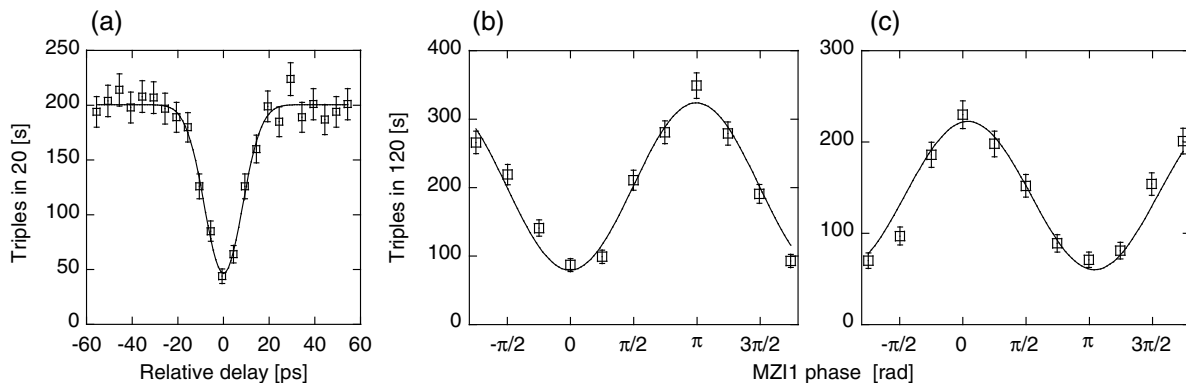


**Fig. 2.** Experimental results for (a) HOM interference and (b), (c) quantum teleportation without transmission fiber. (b) and (c) correspond to the number of triple coincidences in 120 s as a function of MZI1 phase observed by SNSPD3 and SNSPD4, respectively.
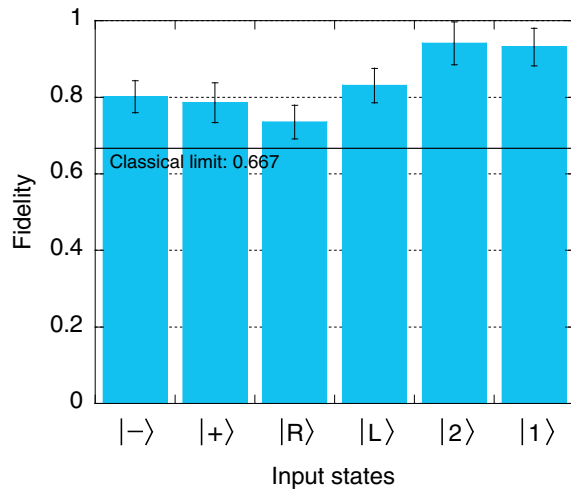
**Fig. 3.** Results of quantum teleportation over 100 km of fiber; experimentally obtained fidelities for six distinct input states.

of heralded single photons were teleported, which required four-fold coincidence measurements rather than the triple coincidence measurements required in our experiment. In addition, the channel losses (including optics losses) of the experiments in [12,13] were around 10 dB larger than those in our experiment. These findings suggest that our quantum teleportation experiment is less efficient than those in [12,13]. This relative inefficiency of our experiment is mainly due to the inefficient coupling of photon pairs to the fiber (∼13%), which is caused by the narrowband filtering of the frequency-correlated photons. The optical losses in our setup and triple coincidence rate of our experiment are described in detail in Supplement 1.

In summary, we have demonstrated the quantum teleportation of a photonic qubit over 100 km of optical fiber. This result confirmed the feasibility of long-distance quantum communication based on quantum teleportation over optical fiber. In addition, we can expect that the highly efficient multifold photon measurement using the SNSPDs will pave the way toward advanced quantum communication systems based on multiphoton quantum states such as the Greenberger–Horne–Zeilinger state [25] and the cluster state [26] over optical fiber.

See Supplement 1 for supporting content.

## REFERENCES

1. N. Gisin and R. Thew, Nat. Photonics **1**, 165 (2007).
2. H. K. Lo, M. Curty, and K. Tamaki, Nat. Photonics **8**, 595 (2014).
3. C. Gobby, Z. L. Yuan, and A. J. Shields, Appl. Phys. Lett. **84**, 3762 (2004).
4. H. Takesue, S. W. Nam, Q. Zhang, R. H. Hadfield, T. Honjo, K. Tamaki, and Y. Yamamoto, Nat. Photonics **1**, 343 (2007).
5. B. Korzh, C. C. W. Lim, R. Houlmann, N. Gisin, M. J. Li, D. Nolan, B. Sanguinetti, R. Thew, and H. Zbinden, Nat. Photonics **9**, 163 (2015).
6. T. Honjo, S. W. Nam, H. Takesue, Q. Zhang, H. Kamada, Y. Nishida, O. Tadanaga, M. Asobe, B. Baek, R. Hadfield, S. Miki, M. Fujiwara, M. Sasaki, Z. Wang, K. Inoue, and Y. Yamamoto, Opt. Express **16**, 19118 (2008).
7. H. J. Briegel, W. Dur, J. I. Cirac, and P. Zoller, Phys. Rev. Lett. **81**, 5932 (1998).
8. N. Sangouard, C. Simon, H. de Riedmatten, and N. Gisin, Rev. Mod. Phys. **83**, 33 (2011).
9. C. H. Bennett, G. Brassard, C. Crepeau, R. Jozsa, A. Peres, and W. K. Wootters, Phys. Rev. Lett. **70**, 1895 (1993).
10. D. Bouwmeester, J. W. Pan, K. Mattle, M. Eibl, H. Weinfurter, and A. Zeilinger, Nature **390**, 575 (1997).
11. A. Furusawa, J. L. Sorensen, S. L. Braunstein, C. A. Fuchs, H. J. Kimble, and E. S. Polzik, Science **282**, 706 (1998).
12. J. Yin, J.-G. Ren, H. Lu, Y. Cao, H.-L. Yong, Y.-P. Wu, C. Liu, S.-K. Liao, F. Zhou, Y. Jiang, X.-D. Cai, P. Xu, G.-S. Pan, J.-J. Jia, Y.-M. Huang, H. Yin, J.-Y. Wang, Y.-A. Chen, C.-Z. Peng, and J.-W. Pan, Nature **488**, 185 (2012).
13. X.-S. Ma, T. Herbst, T. Scheidl, D. Wang, S. Kropatschek, W. Naylor, B. Wittmann, A. Mech, J. Kofler, E. Anisimova, V. Makarov, T. Jennewein, R. Ursin, and A. Zeilinger, Nature **489**, 269 (2012).
14. I. Marcikic, H. de Riedmatten, W. Tittel, H. Zbinden, and N. Gisin, Nature **421**, 509 (2003).
15. F. Bussieres, C. Clausen, A. Tiranov, B. Korzh, V. B. Verma, S. W. Nam, F. Marsili, A. Ferrier, P. Goldner, H. Herrmann, C. Silberhorn, W. Sohler, M. Afzelius, and N. Gisin, Nat. Photonics **8**, 775 (2014).
16. F. Marsili, V. B. Verma, J. A. Stern, S. Harrington, A. E. Lita, T. Gerrits, I. Vayshenker, B. Baek, M. D. Shaw, R. P. Mirin, and S. W. Nam, Nat. Photonics **7**, 210 (2013).
17. V. B. Verma, B. Korzh, F. Bussieres, R. D. Horansky, S. D. Dyer, A. E. Lita, I. Vayshenker, F. Marsili, M. D. Shaw, H. Zbinden, R. P. Mirin, and S. W. Nam, "High-efficiency superconducting nanowire single-photon detectors fabricated from MoSi thin-films," arXiv:1504.02793 (2015).
18. J. Brendel, N. Gisin, W. Tittel, and H. Zbinden, Phys. Rev. Lett. **82**, 2594 (1999).
19. T. Honjo, K. Inoue, and H. Takahashi, Opt. Lett. **29**, 2797 (2004).
20. W. Tittel, J. Brendel, H. Zbinden, and N. Gisin, Phys. Rev. Lett. **84**, 4737 (2000).
21. H. Takesue and Y. Noguchi, Opt. Express **17**, 10976 (2009).
22. C. K. Hong, Z. Y. Ou, and L. Mandel, Phys. Rev. Lett. **59**, 2044 (1987).
23. J. G. Rarity, P. R. Tapster, and R. Loudon, J. Opt. B **7**, S171 (2005).
24. D. F. V. James, P. G. Kwiat, W. J. Munro, and A. White, Phys. Rev. A **64**, 052312 (2001).
25. J. W. Pan, D. Bouwmeester, M. Daniell, H. Weinfurter, and A. Zeilinger, Nature **403**, 515 (2000).
26. P. Walther, K. J. Resch, T. Rudolph, E. Schenck, H. Weinfurter, V. Vedral, M. Aspelmeyer, and A. Zeilinger, Nature **434**, 169 (2005).